Supplementary information for the manuscript entitled "Formation of ring-shaped assembly of microtubules with a narrow size distribution at an air-buffer interface"

Arif Md. Rashedul Kabir,[1] Shoki Wada,[2] Daisuke Inoue,[3] Yoshiki Tamura,[4] Tamaki Kajihara,[4]

Akira Kakugo,[2,5*] Hiroyuki Mayama,[6] Jian Ping Gong,[7*] and Kazuki Sada,[2,5]

[1] Division of Biological Sciences, Graduate School of Science, Hokkaido University, Sapporo 060-0810, Japan

[2] Graduate School of Science, Hokkaido University, Sapporo 060-0810, Japan

[3] Graduate School of Chemical Sciences and Engineering, Hokkaido University, Sapporo 060-0810, Japan

[4] Division of Biological Sciences, Graduate School of Life Science, Hokkaido University, Sapporo 060-0810, Japan

[5] Department of Chemistry, Faculty of Science, Hokkaido University, Sapporo 060-0810, Japan

[6] Nanotechnology Research Center, Research Institute for Electronic Science, Hokkaido University, Sapporo 001-0021, Japan

[7] Faculty of Advanced Life Science, Hokkaido University, Sapporo 060-0810, Japan

*Authors to whom correspondence should be addressed.

E-mail: gong@mail.sci.hokudai.ac.jp; kakugo@sci.hokudai.ac.jp

Telephone/fax: +81-11-706-2774

Free energy arguments of MT-ring formation at an air-buffer interface:

Our system is unique because of the formation of the rings of MTs strongly attached onto the surface by the kinesin motors against ordinary formation of rings and bundles in solution. Here, let us discuss the formation of the ring-shaped MTs at the air-buffer interface from the elongated MTs at the surface of buffer by free energy arguments, while we discussed the formation of bundle of polymer chains in the buffer-solid interface in our previous study,[1] provided that the air-buffer interface and buffer are treated as poor and good solvent conditions for MTs, respectively.

In this discussion, we consider free energies of the elongated state in a good solvent and the ring state in a poor solvent through the intermediate state as shown in Fig. S3, in which we show the observed ring formation processes through Mode 1 and Mode 2. In free-energy arguments, we treat the free energy as the sum of surface energy of elongated and ring MTs, volume energy of a ring, conformation energy, rigidity energy of the ring, Coulomb energy between charges on the coil and translational energy of counterions are distributed around the coil part.

To discuss free energy we define some quantities as follows. Here, the contribution from surface tension is considered by the term surface energy density of the coil and ring, which is energy penalty, is γ and volume energy density in the ring, which is energy gain, is ε_v, where we do not define the volume energy of the coil because of the elongated state. The contour length of a polymer chain attached on surface is L_c (~ 30 μm in experiments) and its diameter is a (a = 25 nm in MTs). On the other hand, the diameter of the ring is $2R_{ring}$ by m-times rounded coil ($m \geq 1$), the diameter of the cross section of the ring d is

$$d^2 \sim ma^2. \qquad (E1)$$

from $\pi(d/2)^2 \sim m\pi(a/2)^2$. The length of the polymer chain in ring part is

$$L_{ring} = 2m\pi R_{ring}. \qquad (E2)$$

The length of the coil part in the intermediate state is

$$L_{coil} = R_{coil}(\text{Mode 1}) = R_{coil1} + R_{coil2}(\text{Mode 2}) = L_c - L_{ring}. \quad (E3)$$

The surface area of the ring part S_{ring} is

$$S_{ring} \sim \pi d \times 2\pi R_{ring} = 2\pi^2 \sqrt{m} a R_{ring}. \qquad \text{(E4)}$$

The volume of the ring part V_{ring} is

$$V_{ring} \sim \pi (d/2)^2 \times 2\pi R_{ring} = \pi^2 m a^2 R_{ring}/2. \qquad \text{(E5)}$$

The surface area of the coil part S_{coil} is

$$S_{coil} \sim \pi a R_{coil}. \qquad \text{(E6)}$$

The number of charges on the coil part is

$$n \sim \pi a L_{coil}/l_B^2. \qquad \text{(E7)}$$

where l_B: Bjerrum length. The charges of the coil part are neutralized by monovalent counterions, while the counterions are condensed onto MT in poor solvent ($n \sim 0$).

Changing R_{coil} with constant L_c and R_{ring}, we describe the free-energy profile in the ring formation. Here, we assumed that the coil part is extended by the kinesin motors as discussed later.

As a result, the free energy G would be described as

$$G \sim \pi^2 a \left(2\gamma\sqrt{m} - \frac{\varepsilon_v m a}{2} \right) R_{ring} + a\gamma R_{coil} + E_{conf} + \frac{\kappa L_{ring}}{R_{ring}^2} + \frac{n_i e^2}{\varepsilon l_B} - \sum_i n_i \ln\left(\frac{V_i}{n_i}\right) \text{ (E8)}$$

where $R_{ring} \sim (L_c - R_{coil})/2m\pi$, $L_{ring} \sim 2m\pi R_{ring}$, the suffix $i = $ coil and ring and $n_i \sim \pi a L_{coil}/l_B^2$ ($n_i \neq 0 (= 0)$ if $L_{coil} \neq 0 (= 0)$) from eq. (E7). The first term is due to the surface and volume energies of the ring, the second term is the surface energy of the coil. The third term is the conformational energy of a polymer chain as[2]

$$E_{conf} = \frac{3}{2}kT[\alpha^2 + \alpha^{-2}]. \qquad \text{(E9)}$$

where kT is thermal energy, α is the size ratio between the polymer chain R and a Gaussian chain R_G in size, $\alpha = R/R_G$. Eq. (E9) means that the Gaussian chain is the most stable state in the conformation energy. R_G in our experiments can be semi-quantitatively determined as shown later. The fourth term in eq. (E8) is the rigidity energy of the ring[3] (κ is the rigidity of a MT filament). The fifth term in eq. (E8)

3

is the Coulomb energy between charges on MT, and the last in eq. (E8) is the translational energy of counterions,[4] V_i and n_i are the free volume and the number of couterions in the coil and ring part, respectively.

Here, we adopt R_{coil} as the variable to draw the G profiles and the parameter change $R_{coil} \rightarrow R$. Since $R_{ring} \sim (L_c - R_{coil})/2m\pi$ and $L_{ring} \sim 2\pi m R_{ring}$, we get

$$G(R) \sim \pi a \left(\frac{\gamma}{\sqrt{m}} - \frac{\varepsilon_v a}{4} \right)(L_c - R) + a\gamma R + \frac{3}{2}kT \left[\left(\frac{R}{R_G} \right)^2 + \left(\frac{R}{R_G} \right)^{-2} \right]$$
$$+ \frac{(2m\pi)^2 \kappa}{L_c - R} + \frac{\pi a R e^2}{\varepsilon l_B^3} - \frac{\pi a R}{l_B^2} \ln \left(\frac{V_{coil}}{n_{ring}} \right).$$

$$(E10)$$

where $V_{coil} \sim a R^2$ on the substrate.

Next, we discuss free energies of the elongated coil (G_{coil}) and ring (G_{ring}) briefly. In the coil state in buffer (good solvent), there are no contributions from the ring, the first and fourth terms in eq. (E10).

$$G_{coil}(R) \sim a\gamma R + \frac{3}{2}kT \left[\left(\frac{R}{R_G} \right)^2 + \left(\frac{R}{R_G} \right)^{-2} \right] + \frac{\pi a R e^2}{\varepsilon l_B^3} - \left(\frac{\pi a R}{l_B^2} \right) \ln \left(\frac{R l_B^2}{\pi} \right).$$

$$(E11)$$

In the ring state at the air-buffet interface (poor solvent), no coil part and the counterions are condensed onto the MT ($n_{ring} \sim 0$), therefore, there are no contributions from the coil, the second, fifth and last terms in eq. (E10).

$$G_{ring}(R) \sim \pi a \left(\frac{\gamma}{\sqrt{m}} - \frac{\varepsilon_v a}{4} \right)(L_c - R) + \frac{3}{2}kT \left[\left(\frac{R}{R_G} \right)^2 + \left(\frac{R}{R_G} \right)^{-2} \right] + \frac{(2m\pi)^2 \kappa}{L_c - R} + G_{coil}(R)$$

$$\sim \pi a \left(\frac{\gamma}{\sqrt{m}} - \frac{\varepsilon_v a}{4} \right)(L_c - R) + \frac{3}{2}kT \left[\left(\frac{R}{R_G} \right)^2 + \left(\frac{R}{R_G} \right)^{-2} \right] + \frac{(2m\pi)^2 \kappa}{L_c - R}.$$

$$(E12)$$

where the last term $G_{coil}(R)$ can be neglected because of the significant difference in the order of the volume and surface energies. From eqs. (E11) and (E12), the free energy profiles can be described as shown in Fig. S4 based on the actual L_c ($\sim$ 30 μm) and l_p ($\sim$ 1 μm). We describe later how R_G is

determined. Fig. S4-(a) shows free energy profile of the elongated coil state, where the elongated conformation is stable. Fig. S4-(b) shows the different paths in the ring formation. While the solid lines are the paths at constant m's with continuous change in radius, the dashed line describes the path of continuous growth of the ring at constant diameter ($2R_{ring}$). Here, it should be noted that there is a size gap between L_c and the initial sizes in the ring formation ($L_c - 2m\pi l_p$) because of nucleation ($2m\pi l_p$ in length).

Effect of kinesin motors: extension energy by the kinesin motors

Contribution of motor protein in the organization of motor protein system was previously discussed elswhere.[1] Here in the Fig. S4, we observe different persistent length, l_p for the elongated MTs in the buffer-solid interface (good solvent) and the ring of MTs at the air-buffer interface (poor solvent), i.e., l_p ~ several tens μm in the former and l_p ~ 1 μm in the latter. As discussed below, it is possible to discuss that the kinesin motors on the substrate fully extend the MT filaments based on the conformational energy in comparison with that of Gaussian chain with no effect of kinesin motors.

Before discussion, the conformational energy E_{conf} [2] is shown again

$$E_{conf} \sim \frac{3}{2} kT(\alpha^2 + \alpha^{-2}). \qquad (E13)$$

where α is the size ratio between a polymer chain (R) and a Gaussian chain (R_G) as

$$\alpha = R/R_G. \qquad (E14)$$

Eq. (E13) represents that Gaussian chain is the most stable state in conformation. Comparing this, the effect is included in R of the elongated state through l_p, as discussed below.

First, let us mention R and R_G, which are directly related with l_p defined by the angular correlation between two unit tangent vectors as[2]

$$s(0) \cdot s(l_p) = \cos\theta \sim 1/e. \qquad (E15)$$

where $s(l)$ is the unit tangent vector at distance l from the start point ($l = 0$) on the reference axis along the polymer chain as shown in Fig. S5. Since $\theta = 68.4° \sim 60°$ from (E15), l_p found in the ring is the order of the radius of ring, now ~ 1 μm. In the ring, the intra-molecular interaction is stronger than the interaction between MTs and the motors, therefore, it would be roughly assumed that the effect of kinesin motors for the ring is smaller or negligible in the ring formation and $l_p \sim 1$ μm in the ring would be defined as the kinesin-free l_p. This point is important in the following discussion about the size of a Gaussian state of MTs.

To estimate R_G of a MT filament, we utilize Kuhn model in which we define Kuhn segment length $l_K = 2l_p$, number of Kuhn segments N_K is $N_K = L_c/l_K$ (L_c is the contour length of MTs and $N_K \geq 1$) and the size of a Gaussian chain $R_G = l_K N_K^{1/2}$.[2] From the size of the ring, it is possible to estimate kinesin-free R_G. Assuming that a typical value that $L_c = 30$ μm and $l_K = 2l_p = 2$ μm, we obtain $N_K = 15$ and $R_G \sim 8$ μm. Thus, we obtain R_G.

Next, let us mention the size of an elongated polymer chain (R) on surface without and with interaction between the chain and surface. Usually, the size of real polymer chains in solution, R is described by the following relation with $\nu = 3/5$.

$$R \sim l_p N_K^{\nu}. \qquad (E16)$$

Here, it should be noted that the rigidity of a polymer chain is reflected in l_p and dimensionality of the system and self-avoiding effect are included in ν. Therefore, the conformational energy is

$$E_{conf} \sim \frac{3}{2} kT \left[\left(\frac{l_p N_K^{\nu}}{R_G} \right)^2 + \left(\frac{l_p N_K^{\nu}}{R_G} \right)^{-2} \right]. \qquad (E17)$$

Very recently, the value of ν of the elongated DNA molecular chains confined in quasi-two dimensional space without the strong interaction between DNA's and the surface has been experimentally reported.[5]

6

In the experiments, v deviates from 3/5 and reaches ~ 0.7 at least. This situation would correspond to that of the elongated MTs on surface without or with the small effect of the kinesin motors. Using $N_K = 15$, $v \sim 0.7$ and $R_G \sim 8$ μm, kinesin-free E_{conf} is roughly expected to be

$$E_{conf} \sim 5kT. \tag{E18}$$

On the other hand, in the elongated MTs with the strong interaction of the motors, l_p (~ 30 μm) is almost equal to the contour length L_c, therefore, $v \sim 1$, $N_K \sim 1$ in eq. (E16). This means that the motors almost fully extend the MTs filaments. E_{conf} of the elongated MTs in comparison with the Gaussian chain is

$$E_{conf} \sim \frac{3}{2}kT\left[\left(\frac{30\times1^1}{8}\right)^2 + \left(\frac{30\times1^1}{8}\right)^{-2}\right] \sim 21kT. \tag{E19}$$

Therefore, the extension energy by the motors E_{ext} is expected to be their difference. As a result, E_{ext} is

$$E_{ext} \sim 21kT - 5kT \sim 16kT. \tag{E20}$$

7

Experimental

Tubulin purification: Tubulin was purified from porcine brain by using a high-concentration 1,4-piperazinediethanesulfonic acid (PIPES; Sigma) buffer (1 M PIPES, 20 mM EGTA, 10 mM MgCl$_2$; pH adjusted to 6.8); high-molarity PIPES buffer (HMPB) and BRB80 buffer were prepared using PIPES and the pH was adjusted using KOH.[6]

Kinesin purification: GFP-fused kinesin-1 construct consisting of the first 560 amino acids (K560-GFP) were prepared as described in previously published papers, by partially modifying the expression and purification methods as follows.[7] For cell lyses of E. coli which expressed K560-GFP, benzonase was added to the buffer to degrade nucleic acids. After binding the proteins to Ni-NTA resin that has affinity to the His-tag of K560-GFP, the resin was washed with a series of buffers of decreasing pH from 8.0 to 6.0 in a step-wise fashion. The target protein was eluted with buffer containing 250 mM imidazole-Cl from the resin. The buffer of eluted samples was exchanged to an MT-binding buffer (25 mM PIPES, 250 mM NaCl, 1 mM EGTA, 2 mM MgCl$_2$, 0.1 mM ATP, 1 mM DTT, pH 6.8 by KOH) using PD-10 column (GE Healthcare). After the buffer exchange, the K560-GFP solution was augmented with 0.5 mM GTP, 4 mM AMPPNP, 0.5 U/ml Apyrase and 10 μM Paclitaxel; hereafter this buffer composition is called MT-binding buffer. The K560-GFP solution (2 ml) was mixed with a MT pellet which was obtained by polymerizing tubulins (25 μM, 1.2 ml) and ultra-centrifugation at 20,000X g for 30 min (37 ˚C), and K560-GFP was bound to MTs by incubating at 25 ˚C for 15 min. The K560-GFP bound MT was ultra-centrifuged at 300,000X g for 30 min (30 ˚C) on an equal volume of cushion buffer which is an MT buffer augmented with 30% (w/v) sucrose. The pellet was suspended with kinesin release buffer (12 mM PIPES, 200 mM NaCl, 2 mM EGTA, 5 mM MgCl$_2$, 5 mM ATP and 10 μM Paclitaxel). After the release of K560-GFP, MTs were removed by ultracentrifuge and the supernatant was yielded as purified K560-GFP which was stored at -80 ˚C after quick freezing in liquid nitrogen.

Rhodamine labeling and stoichiometric estimation: Rhodamine-labeled tubulin was prepared using tetramethylrhodamine succinimidyl ester (TAMRA-SE; Invitrogen) according to standard techniques.[8] The ratio of rhodamine to Tubulin was 1:1, as determined by measuring the absorbance of the protein at 280 nm and the absorbance of tetramethylrhodamine at 555 nm.

Formation of ring-shaped MT assemblies inside the flow cell: Rhodamine-labeled MTs were obtained by polymerizing rhodamine-tubulin in a polymerization buffer (80 mM PIPES, 1 mM EGTA, 5 mM $MgCl_2$, 1 mM guanosine-5′-triphosphate (GTP), 5% DMSO; pH adjusted to 6.8) incubating at 37 ^{0}C for 30 min (molar ratio of Tubulin/rhodamine was 1:1/10; final tubulin concentration was 42 μM). The solution containing the MTs was then diluted with motility buffer (80 mM PIPES, 1 mM EGTA, 2 mM $MgCl_2$, 0.5 mg mL^{-1} casein, 1 mM DTT, 4.5 mg mL^{-1} D-glucose, 50 U mL^{-1} glucose oxidase, 50 U mL^{-1} catalase, 10 μM paclitaxel, and ~1% DMSO; pH 6.8). Flow cells were prepared by placing a cover glass (18 × 18 mm^2; MATSUNAMI) on a slide glass (26 × 76 mm^2) equipped with a pair of spacers to form a chamber of approximately 4 × 18 × 0.1 mm^3 ($W × L × H$) in dimension. A single layer of Parafilm was used to fix the spacer-separated glasses by heating. The flow cell was filled with 0.2 mg mL^{-1} anti-GFP antibody (Invitrogen) following incubation for 15 min and wash with 48 μL of casein solution (80 mM PIPES, 1 mM EGTA, 1 mM $MgCl_2$, ~0.5 mg mL^{-1} casein; pH adjusted to 6.8 using HCl). After incubating for 5 min with casein solution to mask the remaining glass surface, 24 μL of 40 nM K560-GFP solution (~80 mM PIPES, ~40 mM NaCl, 1 mM EGTA, 1 mM $MgCl_2$, 0.5 mg mL^{-1} casein, 1 mM DTT, 4.5 mg mL^{-1} D-glucose, 50 U mL^{-1} glucose oxidase, 50 U mL^{-1} catalase, 10 μM paclitaxel, ~1% DMSO; pH 6.8) were introduced and incubated for 10 min to bind the kinesins to the antibody. The flow cell was washed with 32 μL of motility buffer. A diluted solution (24 μL) of MTs (672 nM in motility buffer) was then introduced and incubated for 10 min, followed by wash with 50 μL of motility buffer. Finally, 24 μL of ATP solution (motility buffer supplemented with 5 mM ATP) containing micro-bubbles (average size 120 μm) formed by extensive pipetting was applied to fabricate MTs. It is to note that the yield of ring formation was found independent of the size of added air bubble.

Formation of MTs ring in the presence of n-hexane: In this experiment, everything was similar to that described in the preceding section except that, before applying the ATP solution an aliquot of n-hexane was passed through the flow cell, after which ATP solution was introduced. Finally microscopic observation was performed at room temperature.

Fluorescence microscopic observation of ring-shaped MT assemblies: Rhodamine-labeled MTs in motility assays were illuminated with a 100 W mercury lamp and visualized by epifluorescence microscopy by using a Plan Apo 60×/1.40 objective (Olympus). Images were captured using a cooled-CCD camera (Cascade II; Nippon Roper) connected to a PC.

In situ observation of the formation of ring-shaped MT assemblies at the air-buffer interface using 'air-buffer interface control system' and 'inert chamber system (ICS)': To perform the in situ observation of MTs-ring formation at the air-buffer interface, motility assay was carried out inside a humidified ICS.[9] The ICS consists of three main parts- a nitrogen gas cylinder, a humidity supporter and the chamber (see Fig. 3). The chamber has two segments- one is the base plate made of stainless steel and the other one is the cover plate made of poly-(methyl methacrylate) (PMMA) (see Fig. 3). The base plate contains the inlet and outlet placed horizontally, which facilitate the passage of nitrogen gas through the chamber and allows the flow rate of nitrogen gas to be controlled. To prevent the MTs from drying and damage by radical oxygen we used ICS during motility assay which was performed inside a glass ring cell (see Fig. 3). Glass ring cell was prepared by placing a glass ring (diameter- 7 mm) on a slide glass (50×40 mm^2) by fixing with glue. Rhodamine-labeled MTs were obtained by polymerizing rhodamine-tubulin in a polymerization buffer (80 mM PIPES, 1 mM EGTA, 5 mM MgCl$_2$, 1 mM guanosine-5′-triphosphate (GTP), 5% DMSO; pH adjusted to 6.8) incubating at 37 °C for 30 min (molar ratio of Tubulin/rhodamine was 1:1/10; final tubulin concentration, 42 μM). The solution containing the MTs was then diluted with motility buffer (80 mM PIPES, 1 mM EGTA, 2 mM MgCl$_2$, 0.5 mg mL^{-1} casein, 1 mM DTT, 4.5 mg mL^{-1} D-glucose, 50 U mL^{-1} glucose oxidase, 50 U mL^{-1} catalase, 10 μM paclitaxel, and ~1% DMSO; pH 6.8). 2.5 μL of 0.2 mg mL^{-1} anti-GFP antibody (Invitrogen) was

dropped into the glass ring cell and incubated for 10 min, followed by a wash with 4 μL of casein solution (80 mM PIPES, 1 mM EGTA, 1 mM MgCl$_2$, ~0.5 mg mL^{-1} casein; pH adjusted to 6.8 using HCl) four times. After incubating for 5 min with casein solution to mask the remaining glass surface, 4 μL of 20 nM K560-GFP solution (~80 mM PIPES, ~40 mM NaCl, 1 mM EGTA, 1 mM MgCl$_2$, 0.5 mg mL^{-1} casein, 1 mM DTT, 4.5 mg mL^{-1} D-glucose, 50 U mL^{-1} glucose oxidase, 50 U mL^{-1} catalase, 10 μM paclitaxel, ~1% DMSO; pH 6.8) was introduced and incubated for 10 min to bind the kinesins to the antibody. The ring flow cell was washed with 4 μL of motility buffer for four times. A diluted solution (4 μL) of MTs (680 nM in motility buffer) was then introduced and incubated for 10 min, followed by washing with 4 μL of motility buffer for four times. Finally, 35 μL of ATP solution (motility buffer supplemented with 5 mM ATP) was applied. After filling the glass ring flow cell with ATP solution, it was set manually inside the inert chamber covering the entire area of the hole at the base plate of chamber and was connected to the micro pump (HARVARD) by capillary tube (GL Sciences, Japan).The glass ring cell and the micro-pump connected together constituted the 'air-buffer interface control system'. The compression spring (see Fig. 3) was then placed upon the flow cell and the chamber was closed. Three main parts of the ICS (nitrogen gas container, humidity supporter and inert chamber) were then connected (series connection) by tube (PharMed BPT). After that, we started passing humid nitrogen gas through the ICS at a flow rate of 10 cm^3/s, keeping the outlet open to 50% (inlet was kept 100% open) and thus removed out the existing oxygen from the chamber. During experiment the humidity inside the inert chamber was maintained more than ~90%. Finally, after passing nitrogen gas for 90 min through the chamber, it was mounted on the stage of a fluorescence microscope placing the hole of the base plate of inert chamber and the 60 × objective facing each other. Prior to this, the 60 × objective was coupled with non-drying immersion oil (Cargille Laboratories). Finally, the buffer solution was pumped out from the glass ring cell at a constant speed (2 μL/sec) to make the air-buffer interface move downward (thickness of the aqueous medium which could induce the MT-ring formation was not studied in this work). Microscopic observation was done at 22–25 ^{0}C

and nitrogen gas was kept passing continuously through the inert chamber until the experiment was finished.

Fluorescence microscopic observation of ring-shaped MT assemblies inside glass ring cell: Rhodamine-labeled MTs in motility assays were illuminated with a 100 W mercury lamp and visualized by epi-fluorescence microscopy by using a Plan Apo 60×/1.40 objective (Nikon). Images were captured using a cooled-CCD camera (iXon; ANDOR) connected to a PC.

Image analysis for motility assays

Movies and images of the motility assays captured by fluorescence microscopy were analyzed to determine the velocity, end-to-end length and contour length of the MTs using image analysis software (Image Pro Plus 6.1J; Media Cybernetics). MTs ring that showed motion over a distance of more than ~0.5 μm, which corresponded to 2 pixels in digital data were judged to rotating MTs ring. To measure the velocity of MTs ring, the track of the MTs in the 6 sequential images with 10 s intervals were manually detected using the software. The measured velocity was the average of the velocity of 50 individual MTs ring, unless mentioned otherwise.

Measurement of flexibility of MTs: At any constant temperature, persistence length could be used as a measure of the flexibility of MTs filaments. In order to determine the persistence length, both the contour length along a filament and the end-to-end distance of the same filament were measured. The persistence length was determined by statistically fitting the data to an equation $\langle R^2 \rangle = 2Lp^2[(L/Lp)-1+\exp(-L/Lp)]$; where $\langle R^2 \rangle$ is the mean squared end-to-end distance, L is the contour length of a filament, and Lp represents the persistence length of filament.[10]

References

(1) Y. Tamura, R. Kawamura, K. Shikinaka, A. Kakugo, Y. Osada, J. P. Gong and H. Mayama, *Soft Matter*, 2011, **7**, 5654.

(2) A. Y. Grosberg and A. R. Khokhlov, *Statistical Physics of Macromolecules*, AIP: New York, 1994.

(3) J. X. Tang, J. A. Käs and J. V. Shah, *Eur. Biophys. J.*, 2001, **30**, 477.

(4) H. Mayama, T. Iwataki and K. Yoshikawa, *Chem. Phys. Lett.*, 2000, **318**, 113.

(5) H. Uemura, M. Ichikawa and Y. Kimura, *Phys. Rev. E*, 2011, **81**, 051801.

(6) M. Castoldi and A. V. Popov, *Protein expression purif.*, 2003, **32**, 83.

(7) R. B. Case, D. W. Pierce, N. Hom-Booher, C. L. Hart and R. D. Vale, *Cell*, 1997, **90**, 959.

(8) J. Peloquin, Y. Komarova and G. Borisy, *Nat. Methods*, 2005, **2**, 299.

(9) A. M. R. Kabir, D. Inoue, A. Kakugo, A. Kamei and J. P. Gong, *Langmuir*, 2011, **27**, 13659.

(10) Y. Arii and K. Hatori, *BBRC,* 2008, **371***,* 772.
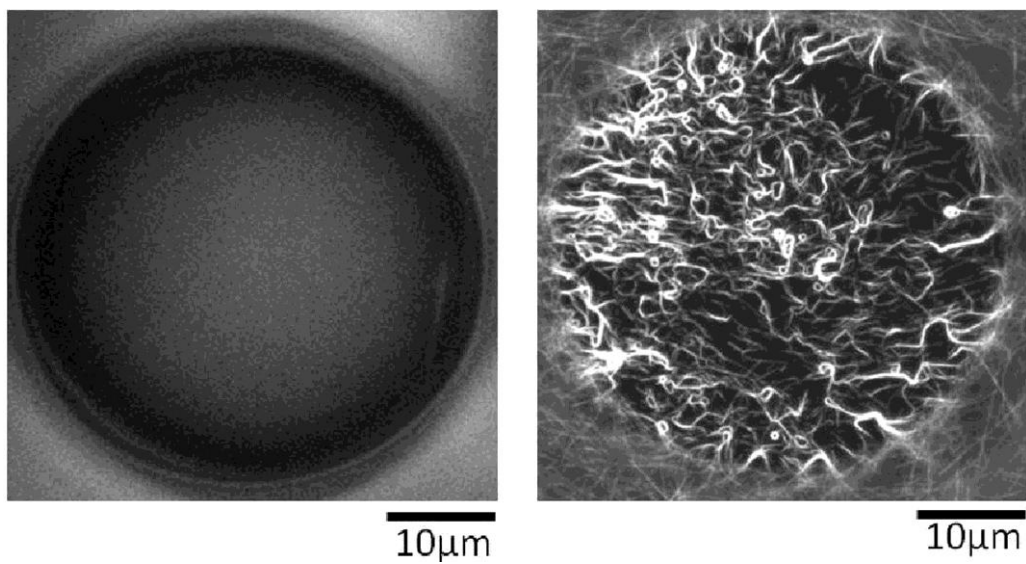
Fig. S1 Image of added air bubble in the motility assay system (left) and effect of air bubble on the

conformational change of filamentous MTs (right).
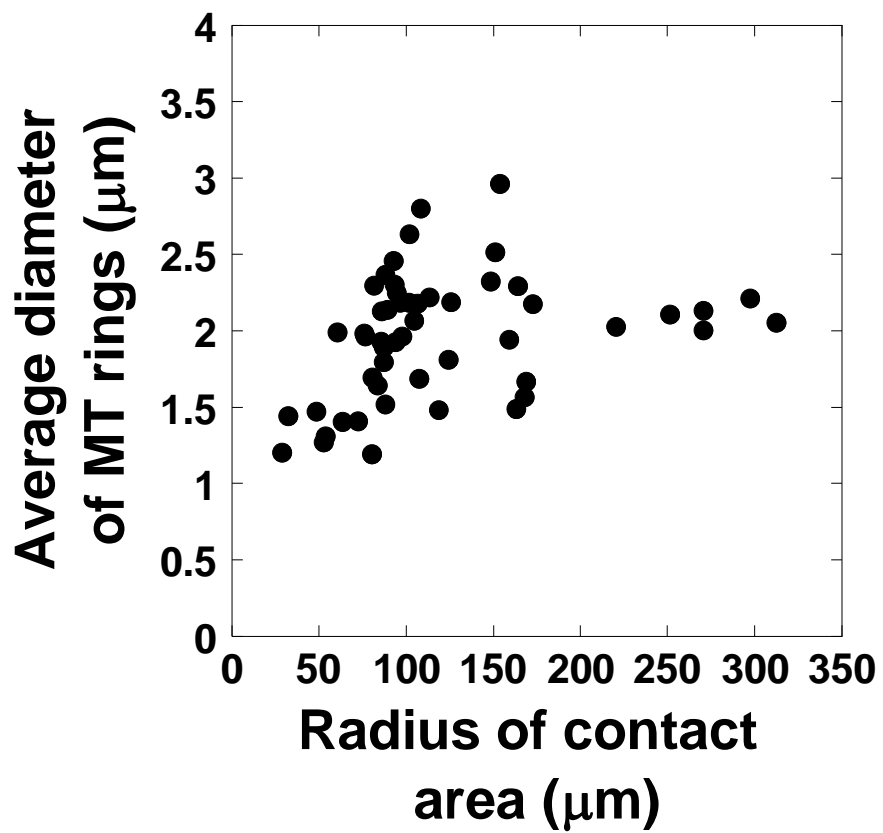
Fig. S2 Effect of air bubble dimension on size of MT rings.
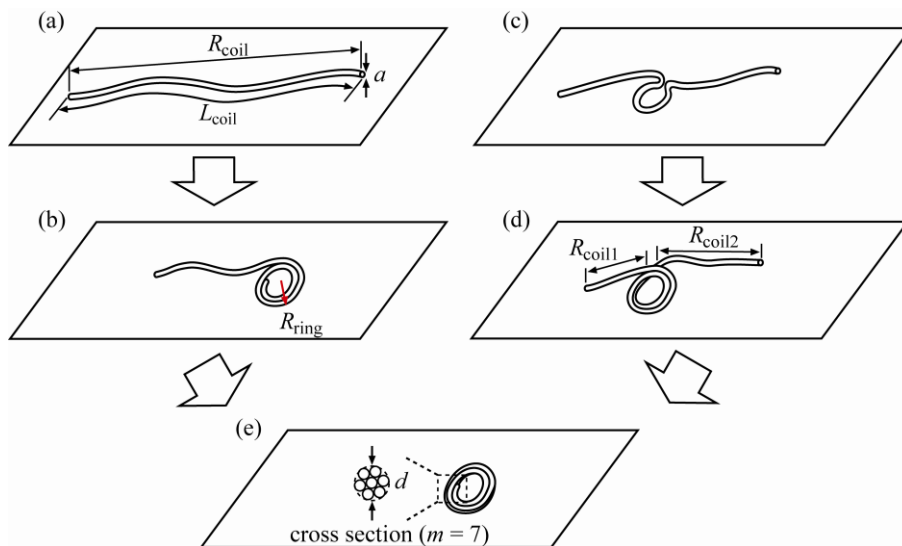
Fig. S3 Schematic representation of the formation of a ring from a coiled polymer chain on a two dimensional surface through Mode 1 ((a) → (b) → (e)) and Mode 2 ((c) → (d) → (e)).
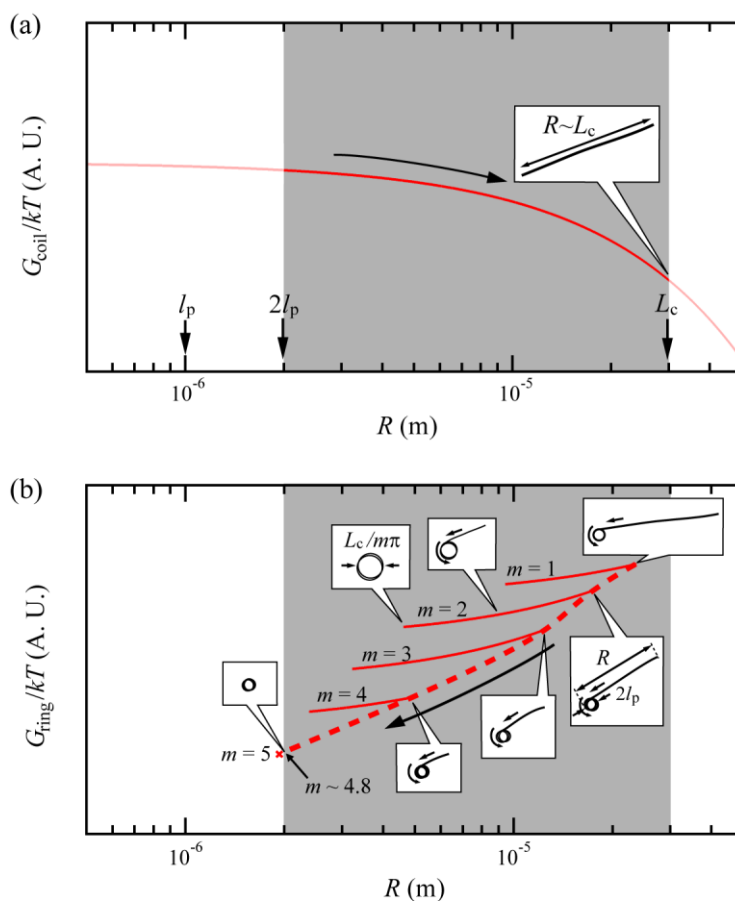
Fig. S4 Schematic representations of the free energy profiles in the coil state (a) and the ring state (b). The shaded areas show the size range from the ring diameter to the contour length based on the actual contour ($L_c \sim 30$ μm) and persistent lengths ($l_p \sim 1$ μm) of a MT filament. In (b), the solid lines from top to bottom are at $m = 1, 2, 3$ and 4, where the gaps from L_c are due to $2m\pi l_p$ and the dashed line represents the path of continuous growth of the ring at a constant diameter.
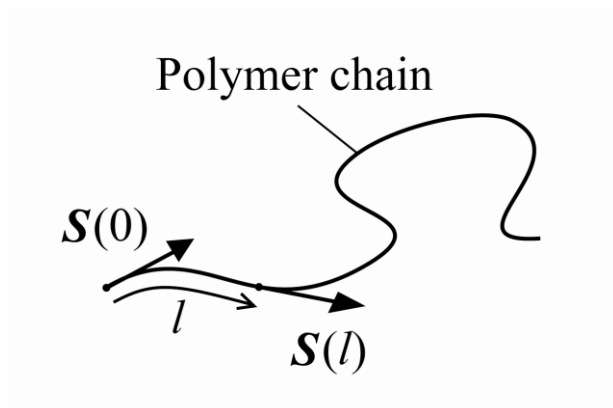
Fig. S5 Schematic representation of unit tangent vectors to define persistent length.
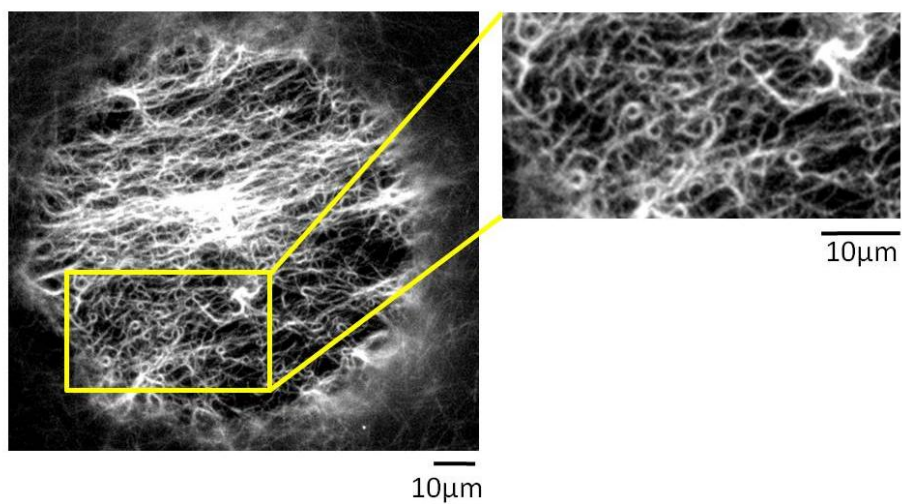
Fig. S6 Effect of n-hexane on the conformational change of filamentous MTs (left); in the presence of n-hexane filamentous MTs underwent ring or bundle formation. Rings formed in the presence of n-hexane are shown in an enlarged image (right).
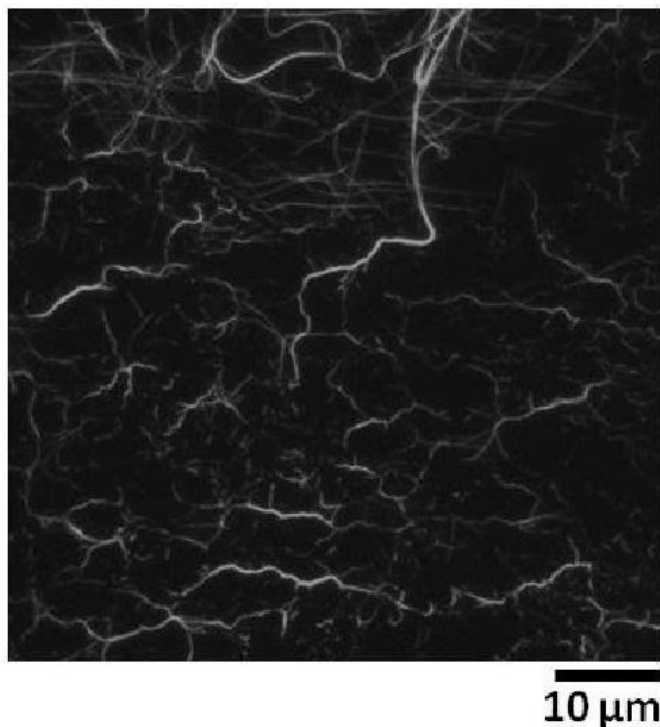
Fig. S7 Image showing the effect of air bubbles on MTs when very low kinesin concentration was used in the motility assay. From this image, it could be observed that in the presence of air bubbles, MTs formed no ring when the kinesin concentration was too low to allow MTs to move.

10μm
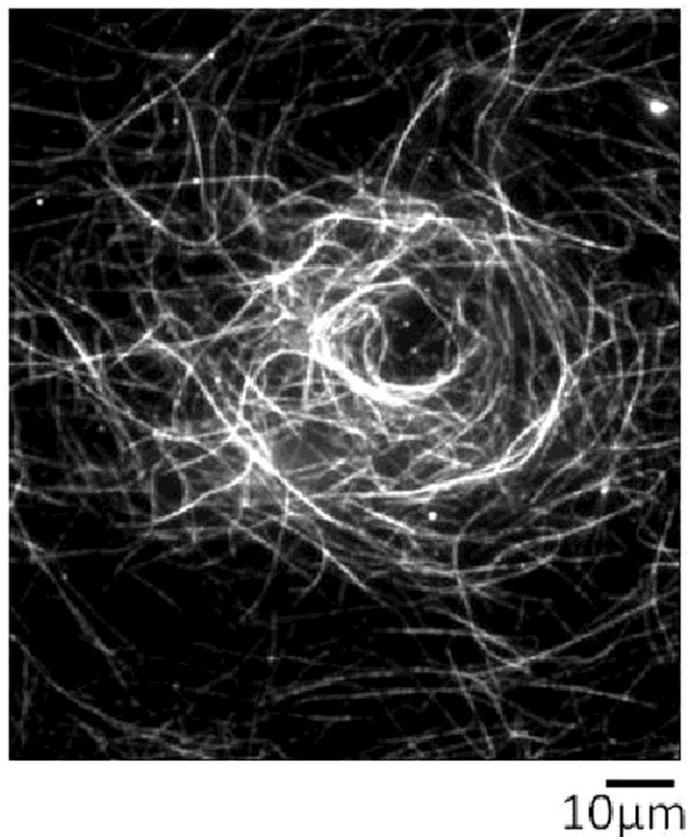
Fig. S8 MTs formed bundles in the presence of added air bubbles when there was no ATP in the motility assay system.
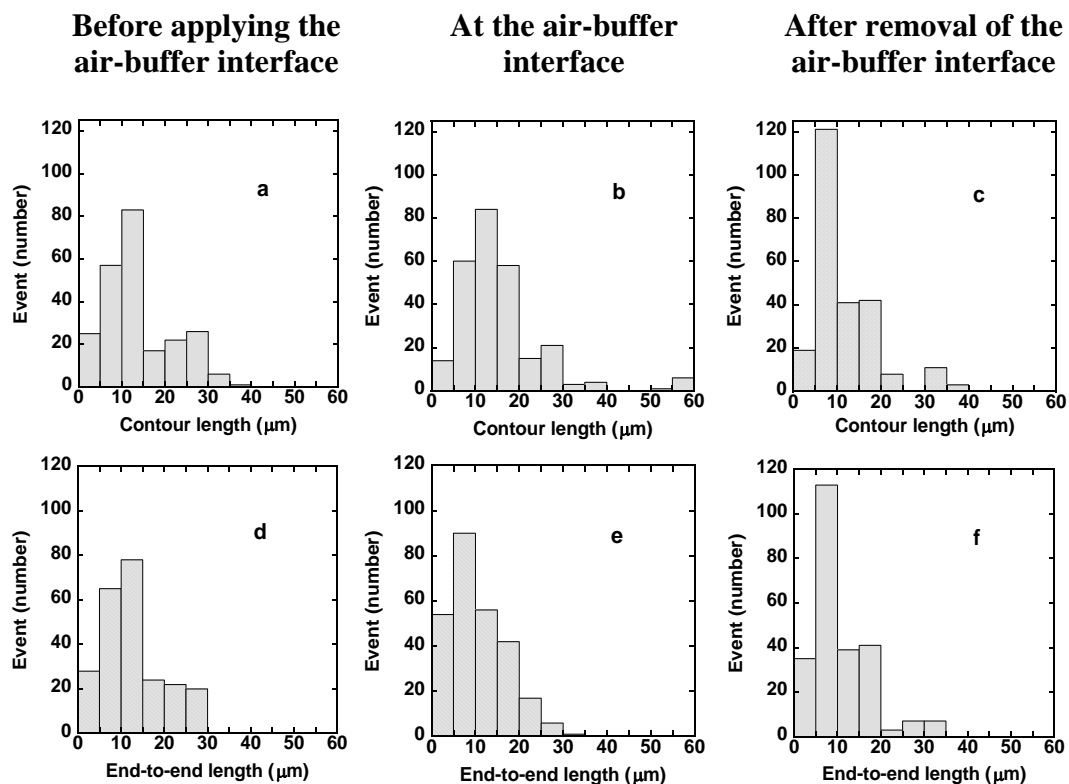
Fig. S9 Distribution of contour length (a, b, c) and end-to-end length (d, e, f) of MTs before applying the air-buffer interface (a, d); at the air-buffer interface (b, e) and after removal of the air-buffer interface (c, f). Average values for the figures are: (a): 13.91 μm; (b): 15.70 μm; (c) 11.80μm; (d) 12.81μm; (e) 10.82μm and (f) 11.92 μm.
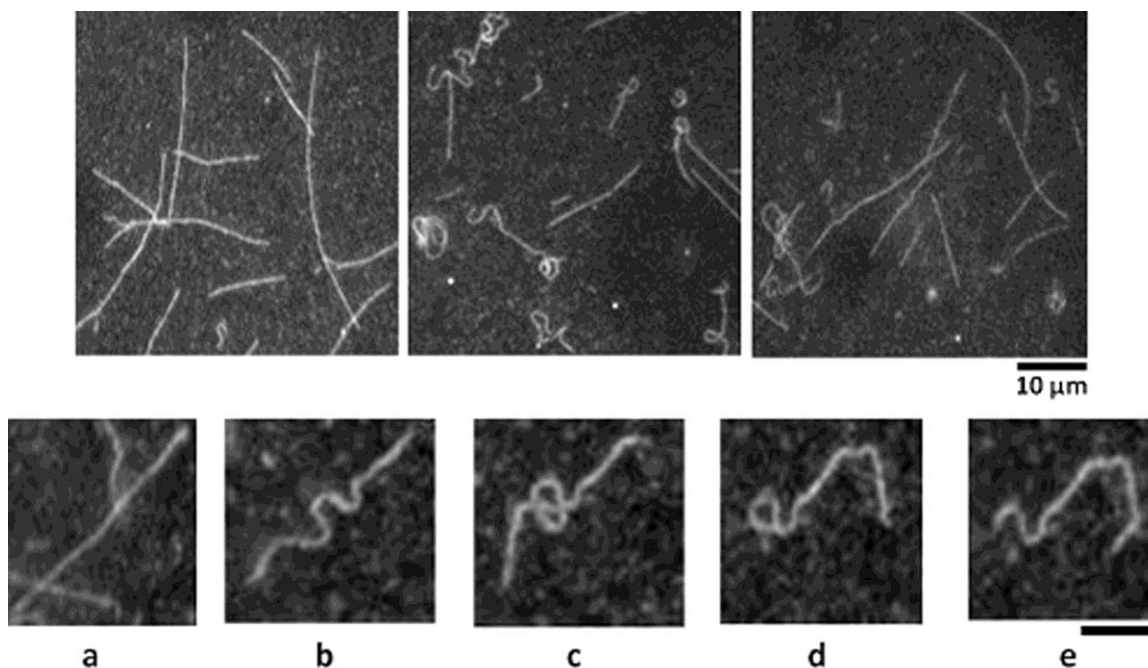
Fig. S10 Reversible change of conformation of MTs depending on the presence or absence of air-buffer interface in the motility assay system. Top: before applying the air-buffer interface (left) all MTs were in linear state; on application of air-buffer interface some of the filamentous MTs started forming ring-shaped structure (middle) and on removal of the air-buffer interface, ring-shaped MTs returned to their original linear state (right). Images were captured at the same field of view. Bottom: a) a linear MT inside the motility assay system, b) the MT started to form loop on application of air-buffer interface in the motility assay system, c) loop formation of the MT was finished d) air-buffer interface was being removed away and s a result, the MT failed to form complete ring; instead loop opening was started in order to return back to the original linear state, e) finally the loop was opened completely and the MT was returning to its original linear state. Scale bar: 5 μm.
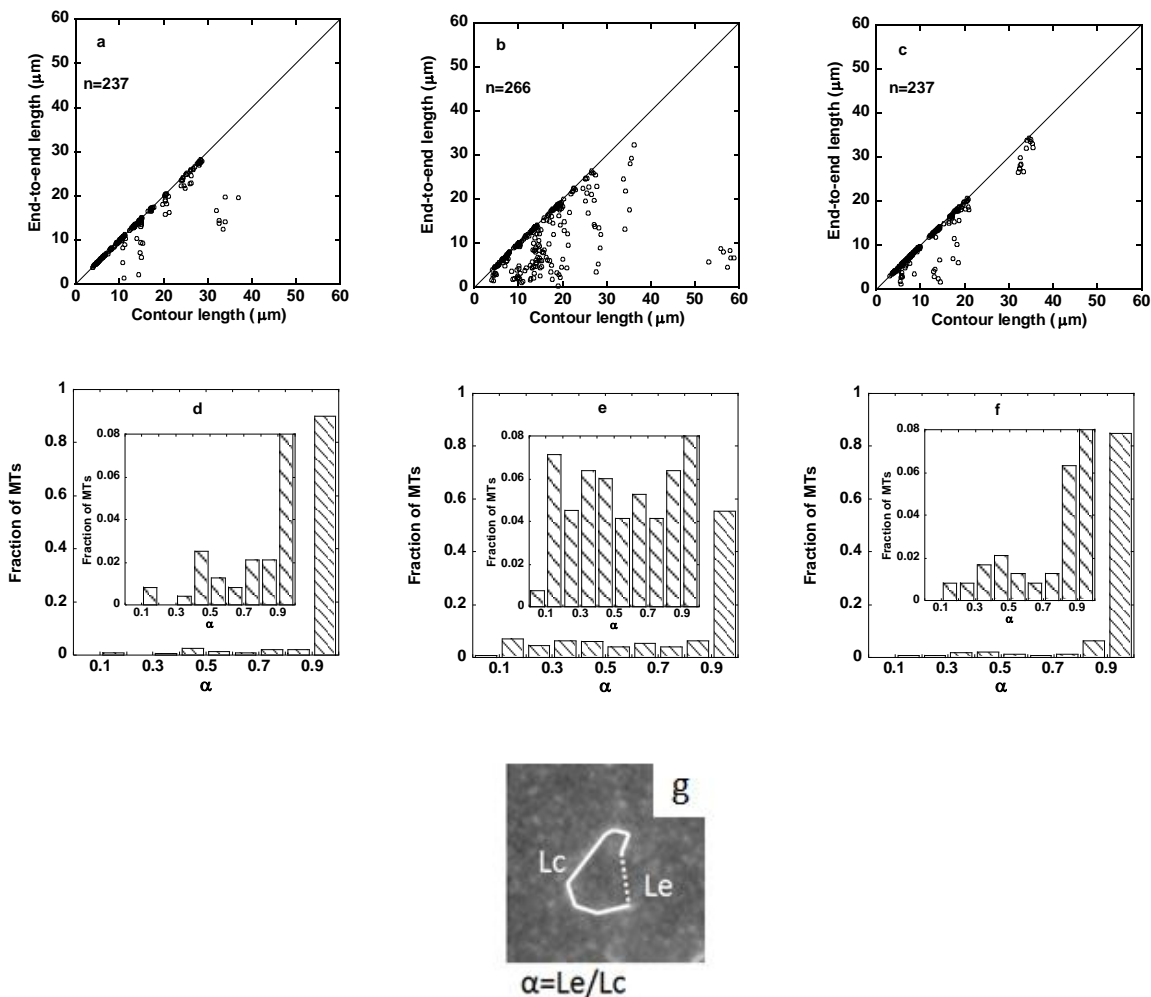
Fig. S11 Plot of the end-to-end length (L_e) and contour length (L_c) of MT filaments: (a) before, (b) after application of air-buffer interface and (c) after removal of the air-buffer interface; 'n' represents the number of sample considered for analysis. Histogram showing the distribution of the ratio of end-to-end length and contour length, α ($\alpha=L_e/L_c$) of MT filaments: (d) before, (e) after the application of air-buffer interface and (f) after removal of the air-buffer interface. Insets show the corresponding magnified expression and $\alpha=1$ is indicated by the straight line in figures (a-c) that correspond to the linear shaped MT filaments. Figure showing the method of measurement of contour length and end-to-end length (g).